

## CHAPTER 3

### Research designs and methods

This chapter describes the research designs and methods of the proposed techniques. The eye gaze tracking system setting is described in section 3.1. Section 3.2 describes the range of applications for eye gaze tracking system setting. The model of eye gaze tracking system and experimental method are described in section 3.3.

The method of image preprocessing is presented from section 3.4 to section 3.5. Section 3.6 describes the eye position detection. Then, the method for iris radius estimation is presented in section 3.7. After both eyes are segmented, the image patch segmentation can be obtained as described in section 3.8.

The proposed method for distance estimation, which includes the uses of the principle of the summation of gray-level intensity of image patch, the principle of the eigenvalues, and the principle of the iris area are described in section 3.9.

Next, the eye gaze center determination is described in section 3.10. The pupil-glint vector computation is discussed in section 3.11. The proposed method of the three-dimensional eye model is described in section 3.12.

Section 3.13 describes the visual angle of eye gaze estimation. How the eye gaze has mapped to the screen coordinate is presented in section 3.14 and how the eye gaze distance is transformed to the computer screen is explained in section 3.15. The screen position used in the experiment is defined as in section 3.16.

### 3.1 Eye gaze tracking system setting

An automatic eye gaze tracking system consisted of a single camera placed in front of the screen. Figure 3.1 shows the configuration of eye gaze tracking system. The IP camera (BOSCH NWC-0900) was utilized to capture eye gaze images. The image sensor was  $6.4 \times 4.8 \text{ mm}^2$  complementary metal oxide semiconductors (CMOS). The screen with the size of 17 inches ( $34 \text{ cm} \times 27 \text{ cm}$ ) was set up on the monitor stand. Figure 3.2 shows the actual eye gaze tracking system.

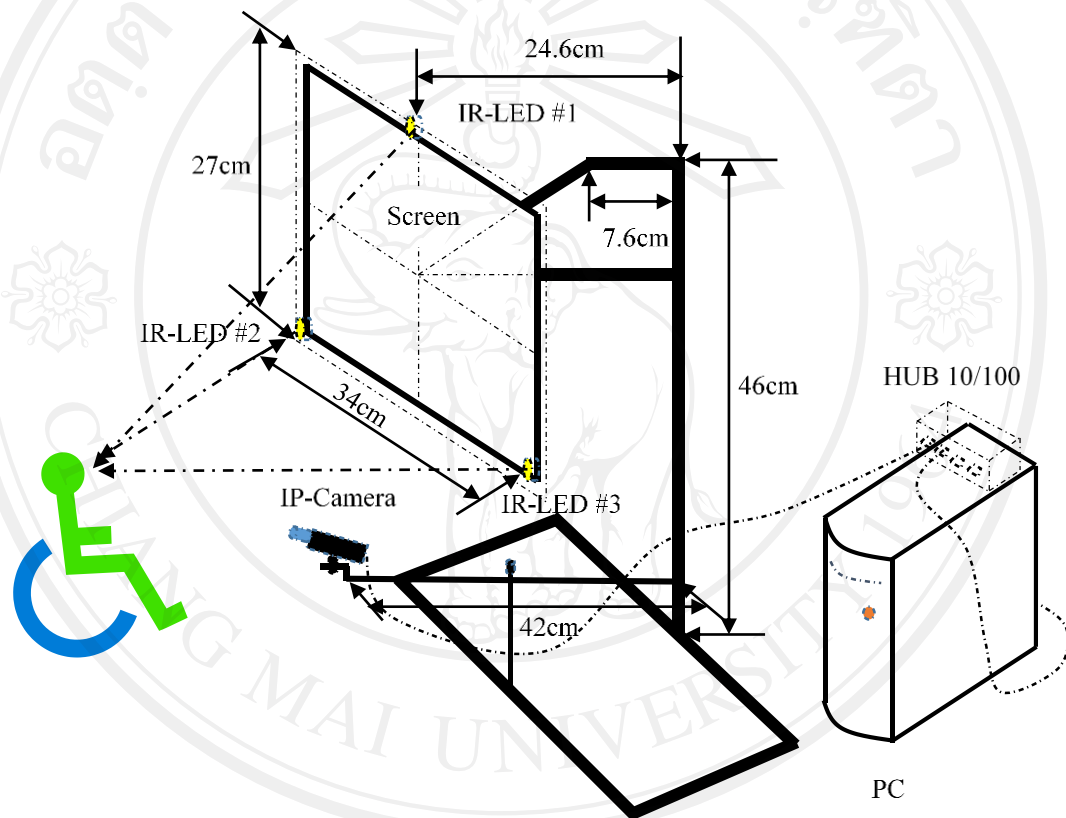


Figure 3.1 Eye gaze tracking system.

ลิขสิทธิ์มหาวิทยาลัยเชียงใหม่  
Copyright © by Chiang Mai University  
All rights reserved



Figure 3.2 Actual eye gaze tracking system.

The eye gaze tracking system used three near-infrared light sources (IR-LEDs), with the wavelength of 850 nm and the diameter of 5 mm, attached to the monitor frame [42]. The 37-mm infrared passed filter was used, which responded to the wavelength of 850 nm covered the C-mount lens. The focal length of C-mount lens was 25 mm. The maximum image resolution was  $1,280 \times 800$  pixels. In addition, the computer Pentium dual-core (E5200) with 2.5 GHz CPU speed and 4 GB RAM was used in the experiment. The IP camera was operated by connecting RJ-45 of the camera cooperated with the 10/100 HUB and Ethernet port of the computer.

The eye gaze tracking system presented in Figure 3.2 was set up with IP camera by placing it 20 cm apart from the screen. The advantage of distance set up was that it could capture the eye gaze images with high resolution. The screen stand for the proposed method was designed as presented in Figure 3.3. Figure 3.4 shows the position of the IP camera installation.

ลิขสิทธิ์มหาวิทยาลัยเชียงใหม่  
Copyright © by Chiang Mai University  
All rights reserved

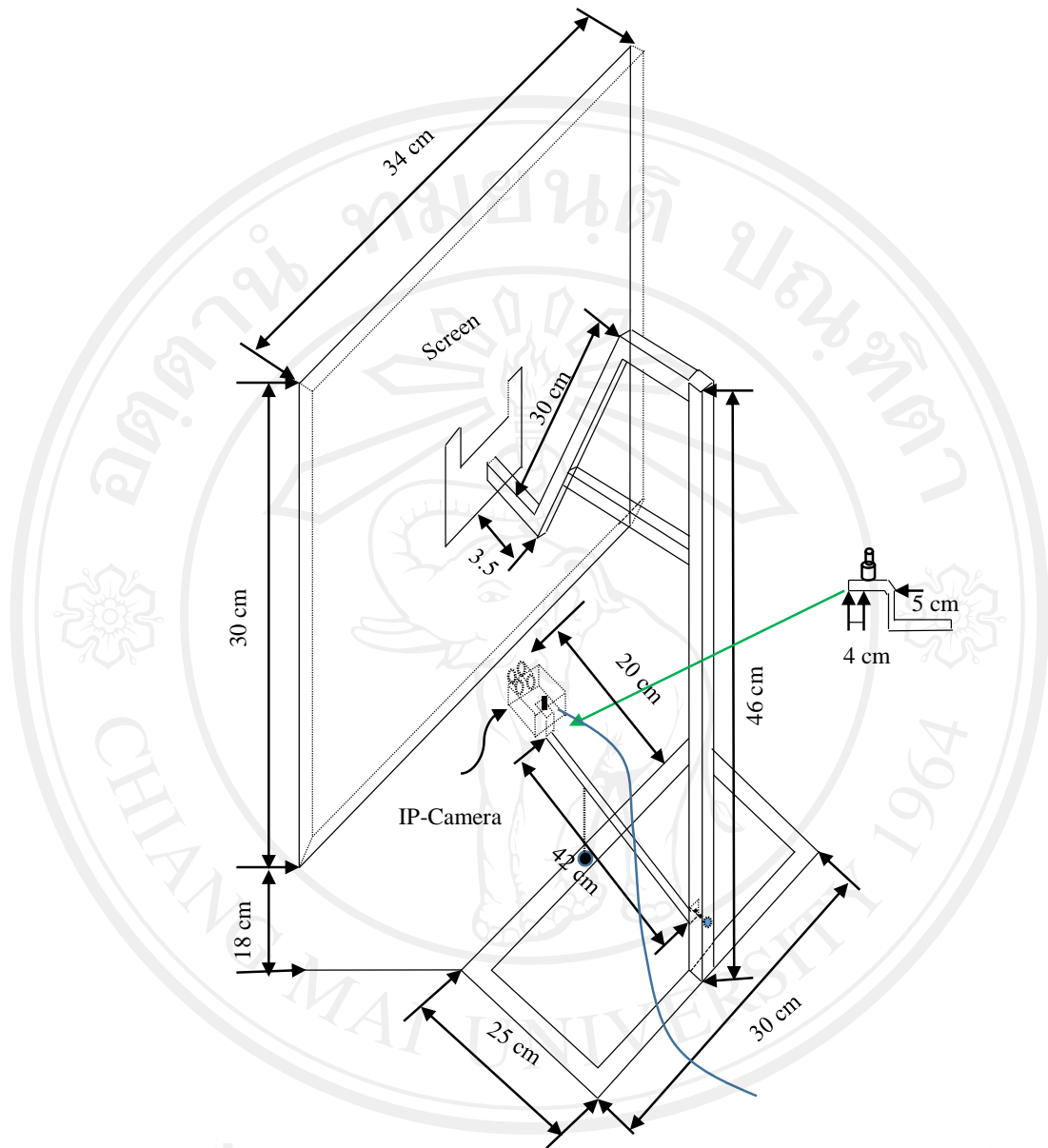


Figure 3.3 Screen stand of the eye gaze tracking system.

ลิขสิทธิ์มหาวิทยาลัยเชียงใหม่  
 Copyright © by Chiang Mai University  
 All rights reserved

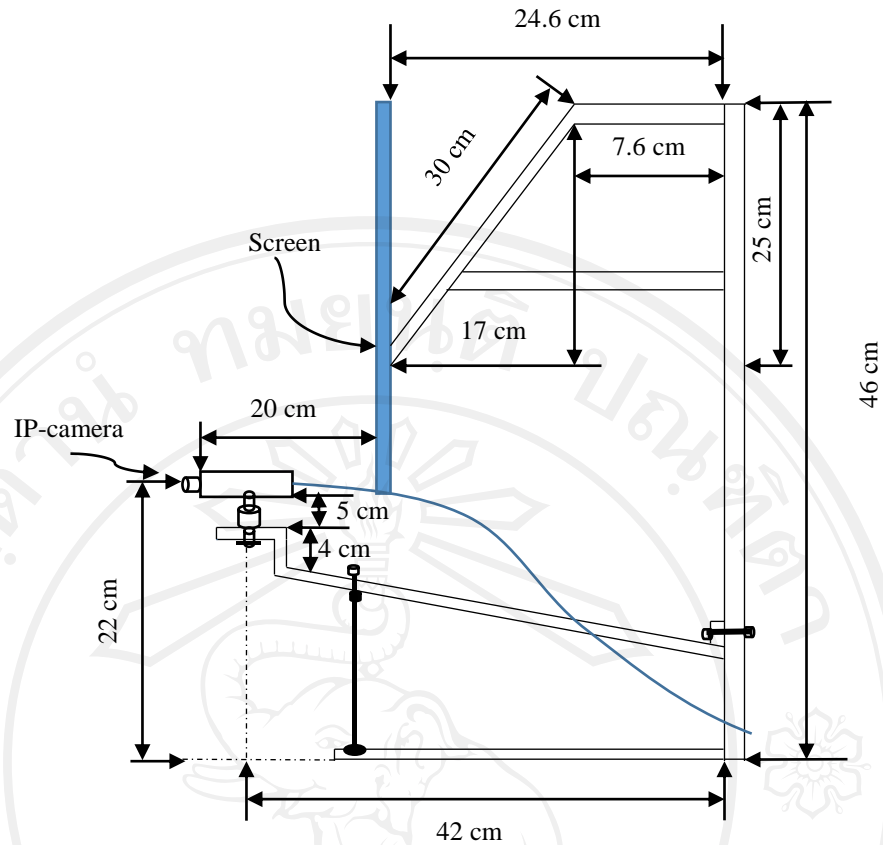


Figure 3.4 Camera position on the screen stand.

Figure 3.5 shows the components of IP camera used in the experiment. Operating modes of the camera to capture the images included day and night modes. In order for the camera to be responsive to the infrared light sources with the wavelength of 850 nm, it was set to the night mode. In addition, the power dissipation of IR-LED was 90 mW, the forward current was 60 mA and the forward voltage was between 1.4 to 1.5 volts. Two IR-LEDs were attached to the bottom of the screen and one IR-LED was located on the top center of the screen frame.

ลิขสิทธิ์มหาวิทยาลัยเชียงใหม่  
 Copyright© by Chiang Mai University  
 All rights reserved

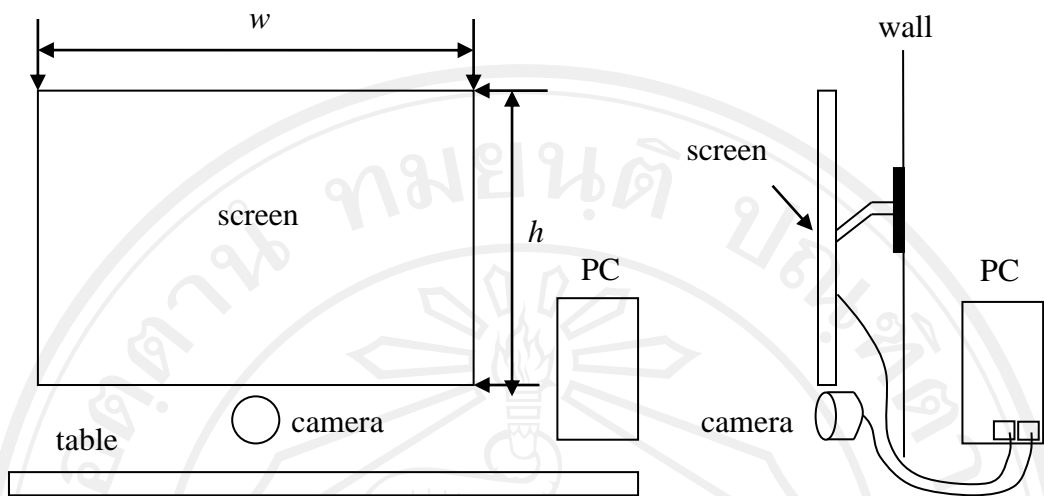


Figure 3.5 Components of IP camera.

### 3.2 Range of applications for eye gaze tracking system setting

The eye gaze tracking system settings as represented in Figure 3.1 through Figure 3.5 were designed to be used for the experiment. On the other hand, for a wide range of the eye gaze tracking system application, the parameters of the screen with respect to the screen width ( $w$ ), screen height ( $h$ ), and the focal length ( $f$ ) of the camera were required for system setting. In addition, the screen was also divided into 10 rows and 6 columns. The camera was set up at the bottom of the screen by placing in front of the screen coordinates. The configuration which describes a wide range application of the eye gaze tracking system setting is shown in Figure 3.6. Two configurations of the system setting were described: the eye gaze system setting on the table, and the eye gaze system setting on the wall.

ลิขสิทธิ์ © by Chiang Mai University  
All rights reserved



(a) Screen placed on the table.

(b) Screen is located on the wall.

Figure 3.6 Eye gaze tracking system for wide range of applications.

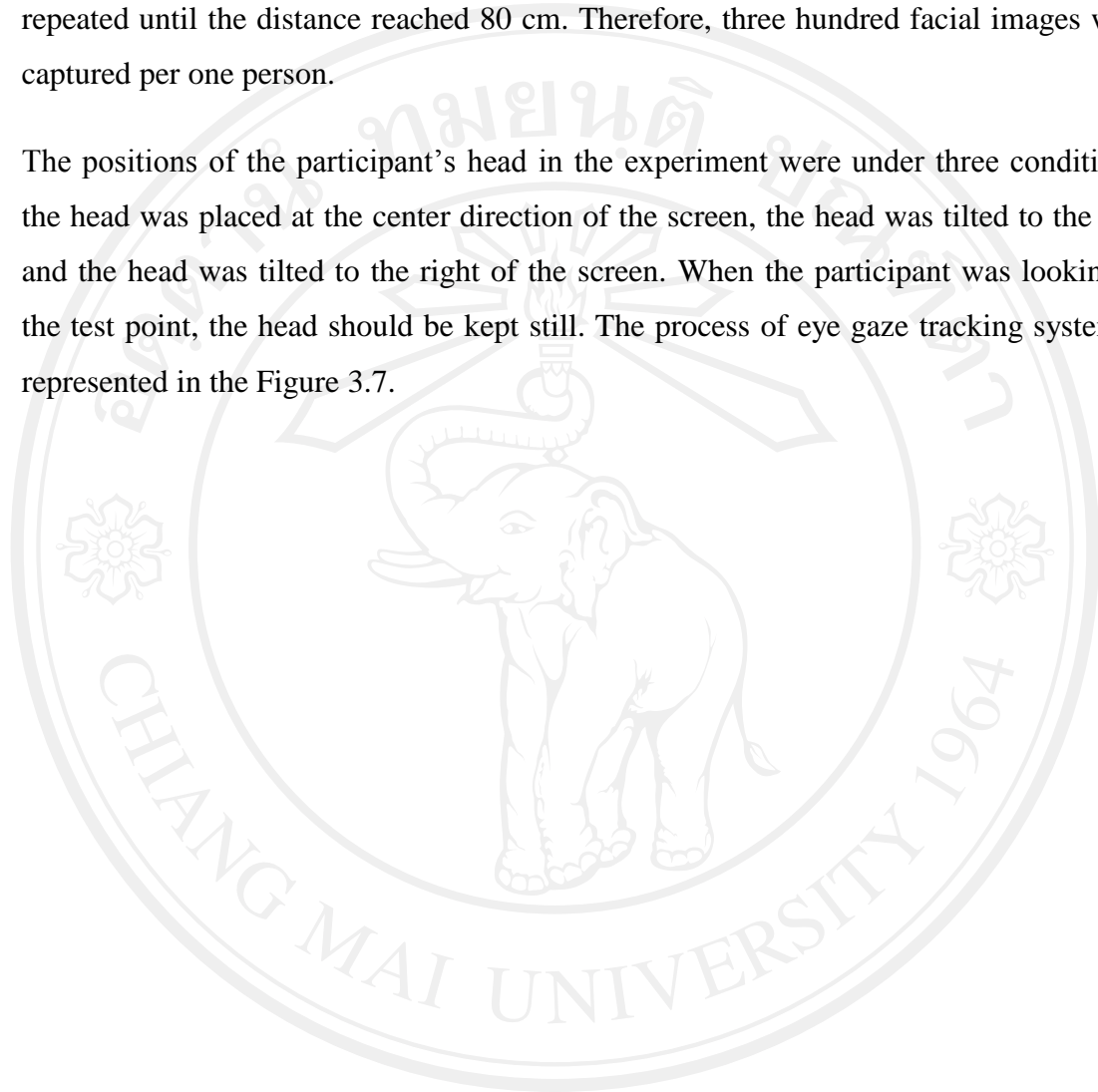
### 3.3 Model of eye gaze tracking system and experiment methods

The proposed method of eye gaze tracking was trained by using a participant for eye gaze distance estimation and tested with 50 participants for eye gaze point on screen estimation, including 31 males and 19 females with ages ranging from 19 to 22 years. The system parameters were required to set up at the first time. The computer screen was divided into 6 rows and 10 columns. Thus, there were 60 predefined test points on the screen. The distance range between the participant's head and the screen in the experiment was 60 to 80 cm.

The experimental method was performed by giving the test point located at the center of the defined area and starting from the top left to the right of the screen. The method for experiment began by letting the participant sit at the distance 60 cm away from the screen. While the system was operating, the participant was told to gaze at the first of test point on the screen. Then, in order to capture the face image, the keyboard was pressed. While image was captured, the participant's head should still be motionless. In order to move the test point passing through the next position, the keyboard

was pressed. The process of image capturing was still working until the participant finished looking at the 60 test points on the screen. Then the images were recorded. After the eye gaze images at the distance of 60 cm had been captured, the participant was asked to move backwards by 5 cm. The procedure of capturing images was repeated until the distance reached 80 cm. Therefore, three hundred facial images were captured per one person.

The positions of the participant's head in the experiment were under three conditions: the head was placed at the center direction of the screen, the head was tilted to the left, and the head was tilted to the right of the screen. When the participant was looking at the test point, the head should be kept still. The process of eye gaze tracking system is represented in the Figure 3.7.



ลิขสิทธิ์มหาวิทยาลัยเชียงใหม่  
Copyright© by Chiang Mai University  
All rights reserved

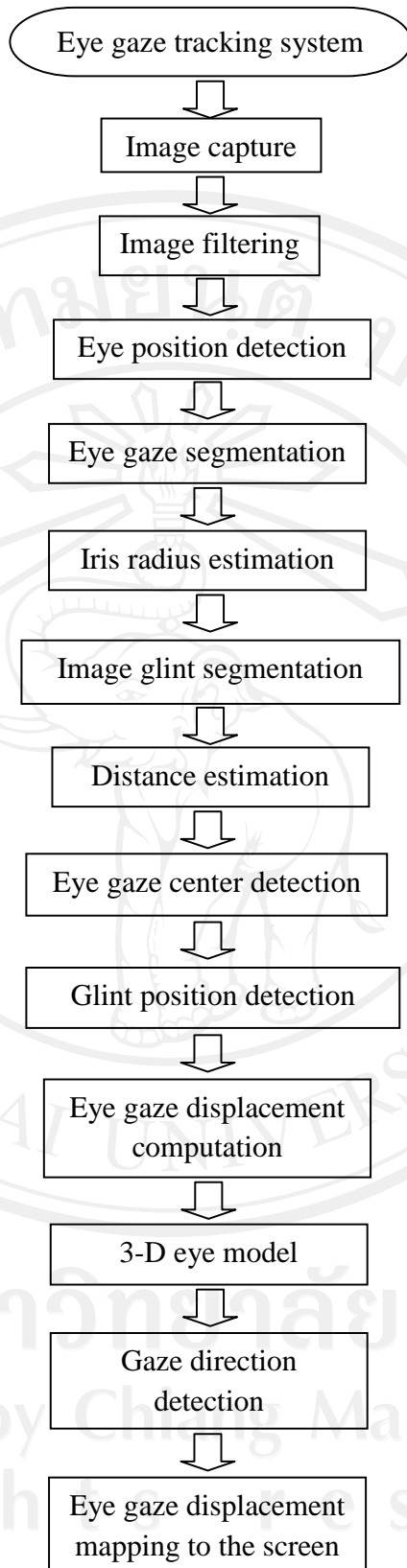
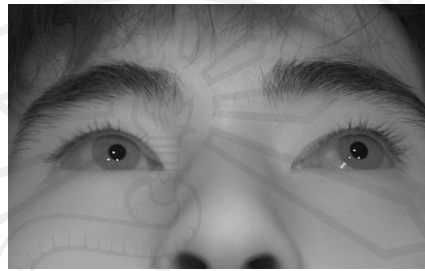


Figure 3.7 Process of eye gaze tracking system.

### 3.4 Image capture

Input images used in the experiment were obtained from a camera with the resolution of  $1,280 \times 800$  pixels. The maximum resolution of the image depends on the camera image sensor efficiency. Both cornea's existences in the image were reflected by IR-LEDs. The examples of captured image under the three conditions of the experiment are shown in Figure 3.8(a) to Figure 3.8(c).



(a) Head placed in the center of the screen.



(b) Head tilted to the left.



(c) Head tilted to the right.

Figure 3.8 Input images for the experiment.

### 3.5 Image filtering

A captured image included the background color and facial features such as eyebrows, nose, and hair. After undesired parts of the features had been filtered, the eye gaze position from which both eye's positions could be easily determined was obtained. The 2-D Gaussian filter was applied to images filtering. The consequence of using the 2-D Gaussian filter for facial image filtering is shown in Figure 3.9.

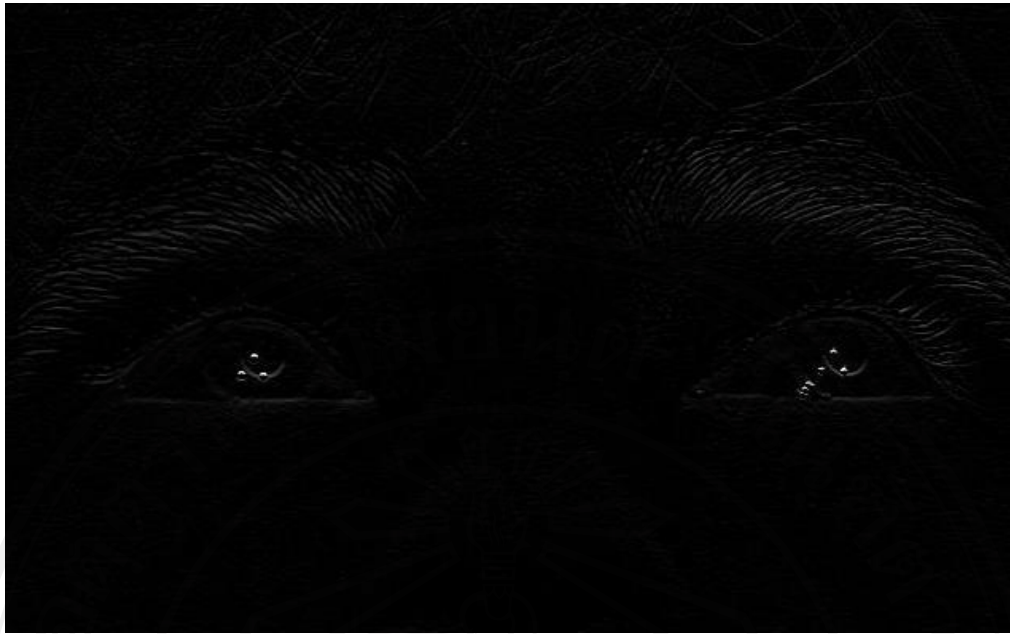


Figure 3.9 Filtered face image.

### 3.6 Eye position detection

Figure 3.9 shows the resulted image obtained from filtering by using Gaussian filter. Both eye positions were determined by using a Blob coloring method which was used for defining the glint positions. Since both eye positions were labeled, the facial image was divided into two parts as shown in Figure 3.10.

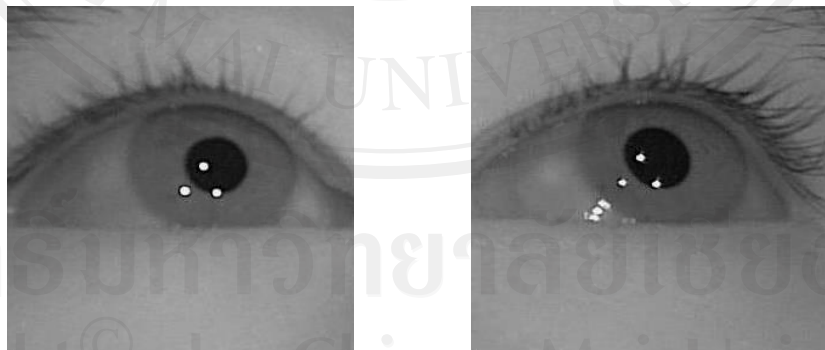


Figure 3.10 Segmented right and left eyes.

### 3.7 Iris radius estimation

The three-dimensional (3-D) eye model required the information of the iris radius which was needed to determine the actual eyeball radius. After both eyes had been segmented, the Hough ellipse was applied for iris radius estimation. The longest line of the iris radius was used for 3-D eye modeling because the longest line of the iris could be obtained even there was an eye movement. In addition, the shortest line of the iris was occluded by the eyelid and eyelashes. The result of the longest line of the iris and the detected iris radius are presented in Figure 3.11.

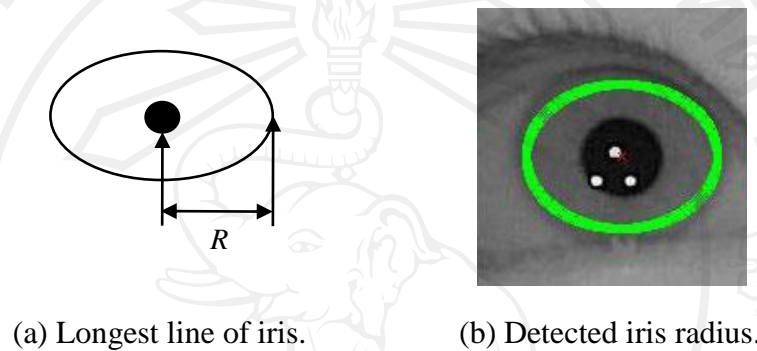


Figure 3.11 Estimated iris's radius.

### 3.8 Image glint segmentation

The cornea was reflected by the three near-infrared light sources as demonstrated in Figure 3.12. The point light sources reflected on the cornea are called 'image glint'. The image glint positions were obtained by applying the Blob coloring to determine the position of the image glint. Then, these glints were segmented from three light sources reflected on the cornea of the eye gaze image as shown in Figure 3.12.

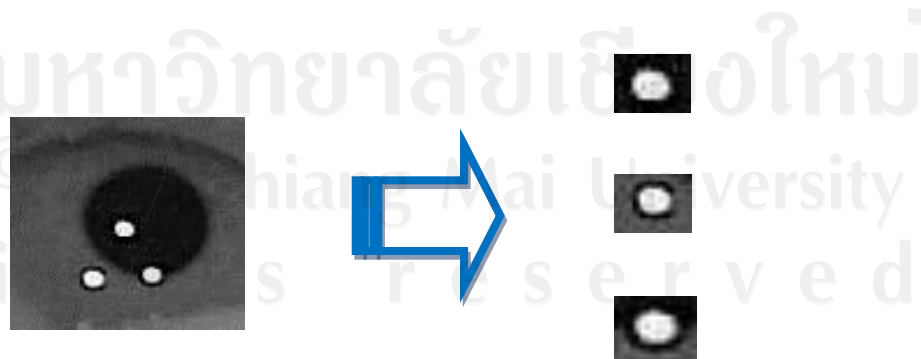


Figure 3.12 Glint detection from three light sources.

### 3.9 Distance estimations

The distance between the participant's face and the computer screen is important for eye gaze tracking system. The performance of the system will decrease if the participant's head position changes accordingly with head movements. Eye gaze distance estimation which uses a single camera is more complicated than other approaches. There are many techniques for distance estimations by a single camera. Most of them require camera calibration. Three proposed methods for eye gaze distance estimations in this system include the method using the summation of gray-level intensity of image patches, the eigenvalues of the iris, and the iris area technique.

#### 3.9.1 Eye gaze distance estimation based on gray-level intensity

This eye gaze tracking system used the principle of the light reflected on the cornea for determining eye gaze positions in an image. The distance between the participant's eye and the screen could be computed by using the characteristic of gray-level intensity of image patch that was irradiated on the cornea image. Intensity of the infrared light sources is inversely proportional to the square of the distance from the source [43]. The density of flux lines is inversely proportional to the square of the distance because the surface area of a sphere increases with the square of the radius. Therefore, the field strength of the flux density is inversely proportional to the square of the distance from the source. The inverse-square law formula is defined as

$$\text{Intensity} \propto \frac{1}{\text{distance}^2} \quad (3.1)$$

The image patch intensity irradiated on the cornea is inversely proportional to the distance between the participant's eye and the screen, according to the relation (3.1). Therefore, by the principle of inverse-square law, the eye gaze distance could be computed by using the quadratic equation of the linear regression method. This proposed method computed the eye gaze distance between the participant's head and the computer screen using the principle of gray-level intensity of the image patch from a single camera with the linear regression method [23].

The gray-level intensity of images patch could be segmented from eye gaze images as shown in Figure 3.13. Image patches were segmented from the images which were taken from a distance ranging from 60 to 80 cm for computing the eye gaze distance function.

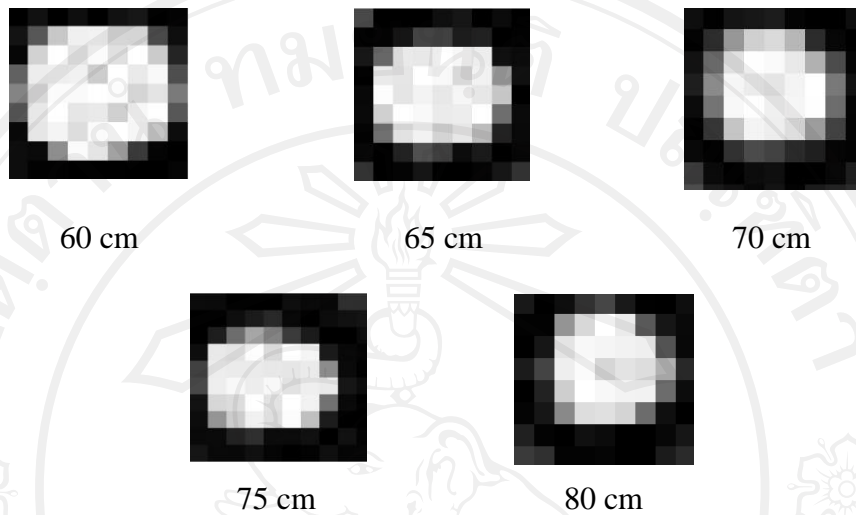


Figure 3.13 Image patches at different distances.

The linear least squares, least squares second order polynomial, and power regressions were applied for eye gaze distance estimation function. The image patches intensity greater than 100 were used for computing the eye gaze distance equation. The summation of gray-level intensity of the image patches then was used as an input to the third regression. Table 3.1 shows an example of the summation of gray-level intensity of the image patches.

Table 3.1 Example of image patches intensity.

Patches number	Distance ranges				
	60 cm	65 cm	70 cm	75 cm	80 cm
1	10757	8161	7728	6916	5880
2	10490	9380	7652	6132	5395
3	10890	9473	7237	6488	5872
4	10262	8802	7998	6226	5834

The results of eye gaze distance estimation using the linear least squares is presented as

$$y = -0.004739x + 108.043821. \quad (3.2)$$

The eye gaze distance estimation using the least squares second order polynomial can be modeled as

$$y = 132.95978 - 0.01199x + 0.0000004878x^2. \quad (3.3)$$

In addition, for the power regression, the eye gaze distance estimation is

$$y = 2733.3x^{-0.411} \quad (3.4)$$

where  $y$  refers to the eye gaze distance and  $x$  refers to the summation of gray-level intensity of the image patch.

Equations (3.2) to (3.4) are obtained by using the summation of gray-level intensity of the image patch of the participant. Then, these equations were tested on five participants in order to evaluate the eye gaze distance accuracy. The results of eye gaze distance estimation by the linear least squares method are demonstrated in Table 3.2, showing mean average distance and mean absolute error (MAE). Table 3.3 represents the percent of accuracy of the linear least squares. Figure 3.14 shows estimated distance by using the linear least squares method.

Table 3.2 Distance estimation using the linear least squares.

	Linear least squares				
	60 cm	65 cm	70 cm	75 cm	80 cm
Mean average distance (cm)	62.75	63.40	71.80	78.31	81.51
MAE (cm)	2.34	2.50	2.16	3.35	2.14

ลิขสิทธิ์มหาวิทยาลัยเชียงใหม่  
Copyright © by Chiang Mai University  
All rights reserved

Table 3.3 An accuracy of the linear least squares.

Volunteers	Percent accuracy (%)				
	60 cm	65 cm	70 cm	75 cm	80 cm
Participant 1	92.70	96.44	95.63	94.49	98.07
Participant 2	96.37	94.59	95.31	96.36	97.86
Participant 3	93.65	94.39	95.56	95.93	96.10
Participant 4	92.81	96.64	97.88	96.50	97.73
Participant 5	93.24	94.63	95.36	95.76	95.13

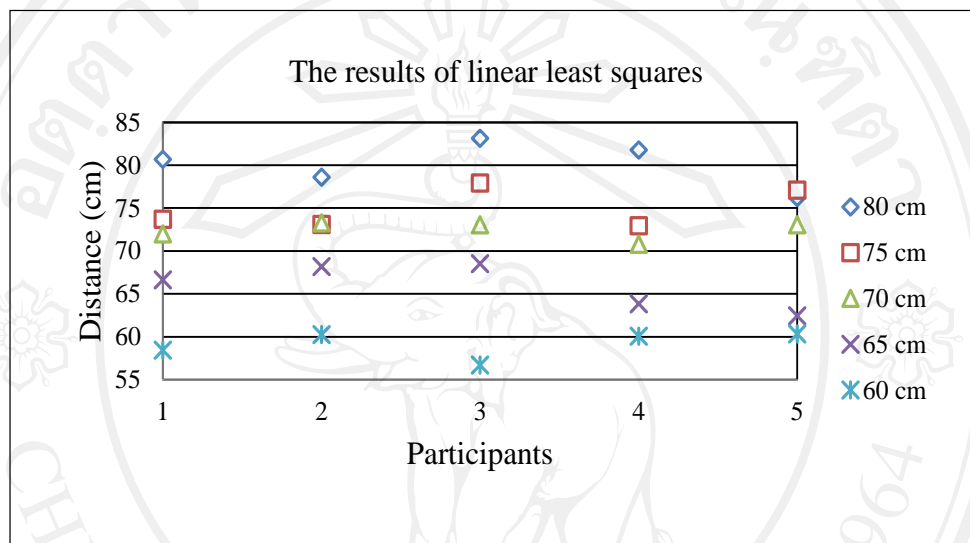


Figure 3.14 Estimated distance using the linear least squares.

For the least squares second order polynomial method, the results of eye gaze distance estimation are shown in Table 3.4 and Figure 3.15.

Table 3.4 Distance estimation using least squares second order polynomial.

	Least squares second order polynomial				
	60 cm	65 cm	70 cm	75 cm	80 cm
Mean average distance (cm)	62.70	63.44	69.90	77.01	81.25
MAE (cm)	2.09	1.93	1.61	2.33	2.37

Table 3.5 An accuracy of least squares second order polynomial.

Volunteers	Percent accuracy (%)				
	60 cm	65 cm	70 cm	75 cm	80 cm
Participant 1	99.03	97.73	96.15	94.76	97.97
Participant 2	96.97	96.70	97.53	94.36	96.54
Participant 3	98.53	96.64	97.86	97.07	95.64
Participant 4	95.51	97.37	97.91	94.43	97.89
Participant 5	96.05	96.16	96.76	94.95	93.17

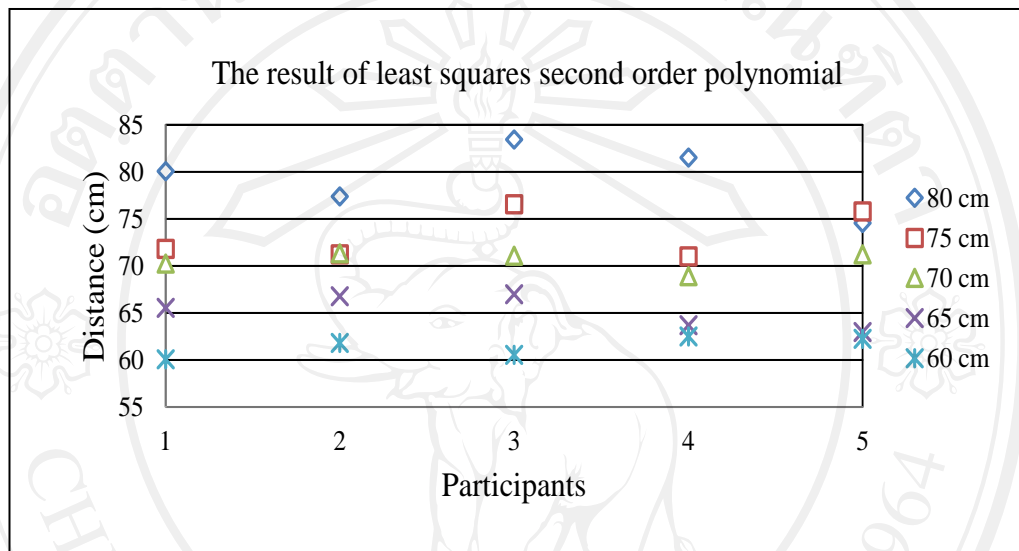


Figure 3.15 Estimated distances using least squares second order polynomial.

Similarly, the results of eye gaze distance estimation by the power regression method are demonstrated in Table 3.6 to Table 3.7.

Table 3.6 Distance estimation using power regression.

	Least squares second order polynomial				
	60 cm	65 cm	70 cm	75 cm	80 cm
Mean average distance (cm)	61.56	66.72	70.66	71.94	79.20
MAE (cm)	2.17	2.47	2.17	3.60	2.61

Table 3.7 An accuracy of power regression.

Volunteers	Percent accuracy (%)				
	60 cm	65 cm	70 cm	75 cm	80 cm
Participant 1	96.88	97.93	96.37	94.45	96.77
Participant 2	96.69	96.92	98.30	93.67	94.42
Participant 3	97.71	96.85	98.48	97.86	97.79
Participant 4	95.84	97.65	97.74	93.64	98.52
Participant 5	94.80	91.62	93.63	96.40	96.21

The average accuracy of eye gaze distance estimation of the linear least squares was 95.64%, while the average accuracy of the least squares second orders polynomial was 96.54%. For the power regression, the average accuracy of eye gaze distance estimation was 96.29%. All equations were constructed from a single image patch from the right eye image of a participant. However, the distance range availability depends on the image sensor resolution.

### 3.9.2 Eye gaze distance estimation based on eigenvalues of iris

Although the eye gaze distance estimation was achieved by using the summation of gray-level intensity of the image patches, the distance measurement was still a problem. According to the theory of the inverse-square law, the intensity is inversely proportional to the quadratic distance. However, there was an alternative method for eye gaze distance estimation by using the principle of the eigenvalues of an ellipse. The proposed method for eye gaze distance estimation was the one which used the principle of eigenvalues of an ellipse. The eye gaze images for training the system were obtained from the participant's eye. It was assumed that the iris is an elliptical shape and therefore the Hough ellipse transforms method was used. The eigenvalues were obtained by using the major and minor axes lengths of the ellipse. The eye gaze distance equation by the eigenvalue technique was evaluated by the regression method (linear, exponential, logarithmic, and power regressions).

## 1) Eigenvalue computation from iris

The eye gaze image was segmented by using the Hough ellipse transform. The iris image was defined as the function  $f(x, y)$  of two real variables  $x$  and  $y$ . This function can be divided into  $N$  rows and  $M$  columns. In order to determine the eigenvalues of an image  $f(x, y)$ , the segmented iris was used for computing the eigenvalues of an ellipse iris. The process for computing the eigenvalue is described as follows:

Step 1: Transform the iris image into a 2-D gray scale image.

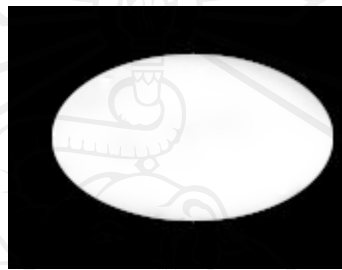


Figure 3.16 Region of interest.

Step 2: Compute the vector of iris region.

Step 3: Construct the covariance matrix.

Step 4: Compute the eigenvalues of the iris region.

## 2) The proposed method

### 2.1) Iris segmentation

The iris image could be segmented by using the Hough ellipse transform. The inner iris ellipse was used for computing the vector. The results from segmenting of the iris image are presented in Figure 3.17.

ลิขสิทธิ์ © by Chiang Mai University  
All rights reserved

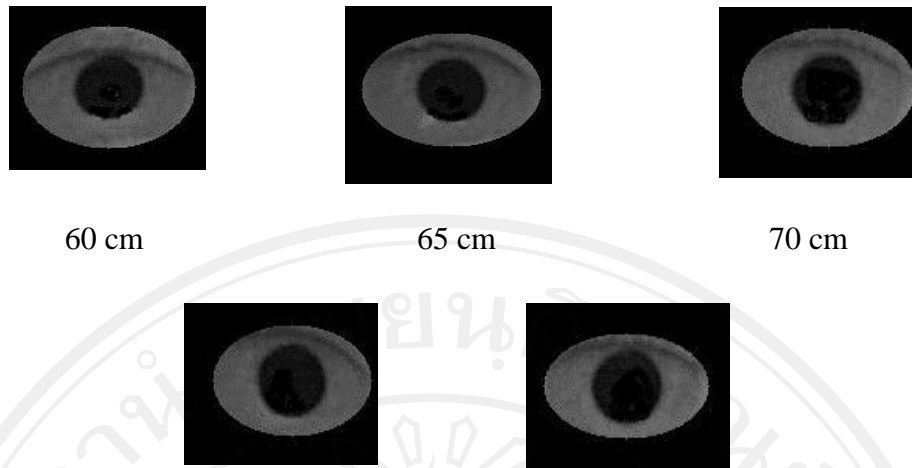


Figure 3.17 Sample segmented irises.

## 2.2) Computation the eye gaze distance estimation equation

The results of segmented iris images are shown in Figure 3.17. The eigenvalues of the iris images were then computed. An example of the results of the eigenvalues computation which used an image taken at a distance of 60 cm are presented in Table 3.8. In order to construct an equation of the eye gaze distance estimation, the summation of eigenvalues of major and minor axes of the iris was used for training the system. The eye gaze distance equation was obtained from the eye image of a participant. The results of eigenvalue summation from a distance of 60 to 80 cm with an increment of 5 cm are demonstrated in Figure 3.18.

Table 3.8 Example of eigenvalues of the iris.

Images No.	Eigenvalues of the iris			
	Distance	Minor axis	Major axis	Summation
1	60 cm	503.81	1329.69	1833.51
2	65 cm	502.77	1009.42	1512.19
3	70 cm	282.12	1074.13	1356.25
4	75 cm	263.23	828.35	1091.59
5	80 cm	233.43	745.31	978.75

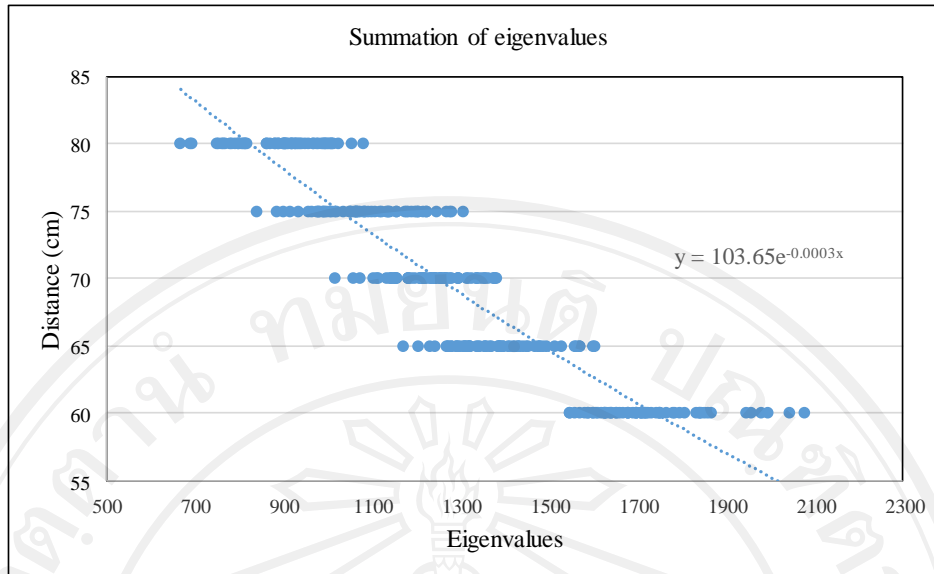


Figure 3.18 Summation eigenvalues of an iris.

Figure 3.18 shows the results of summation eigenvalues of an iris from the iris images. From the figure, the training set was modelled by the exponential regression. The training result of the exponential regression formula is defined as

$$y = 103.65e^{-0.0003x} \quad (3.5)$$

where  $y$  is the eye gaze distance and  $x$  is the eigenvalues of the iris.

### 2.3) The experimental results

The eye gaze distance equation by the exponential method was tested on 30 participants. The subjects were sitting at a distance ranging from 60 to 80 cm and look at 60 predefined points on the screen. The proposed method performance was required to evaluate accuracy, mean average of distance, mean absolute error (MAE), and standard deviation (SD). In addition, the proposed method was compared to the other regressions (linear, logarithmic, and power regressions) methods. The experimental results obtained by using the exponential regression are represented in Table 3.9.

Table 3.9 Results of distance estimation using exponential regression.

	Estimated distances					
	60 cm	65 cm	70 cm	75 cm	80 cm	Average
Accuracy (%)	96.10	96.55	96.68	97.08	97.04	96.69
MAE (cm)	2.40	2.26	2.35	2.24	2.39	2.33
SD (cm)	2.89	2.80	2.83	2.75	2.85	2.82

	Estimated distances				
	60 cm	65 cm	70 cm	75 cm	80 cm
Mean average distance (cm)	59.96	64.89	70.60	75.00	79.15

The test results of the exponential equation showed 96.69% maximum accuracy, 2.33 cm mean average error (MAE), and 2.82 cm standard deviation.

In the same manner, the summation of eigenvalues of the iris was used to construct the eye gaze distance estimation equation for the linear regression. The solution of the equation is represented in (3.6). The test results by using the linear regression are shown in Table 3.10.

$$y = -0.0218x + 97.524 \quad (3.6)$$

where  $y$  is the eye gaze distance and  $x$  is the eigenvalues of the iris.

Table 3.10 Results of distance estimation using linear regression.

	Estimated distances					
	60 cm	65 cm	70 cm	75 cm	80 cm	Average
Accuracy (%)	94.08	95.64	96.61	96.95	96.62	95.98
MAE (cm)	3.57	2.89	2.46	2.32	2.68	2.78
SD (cm)	4.11	3.44	2.92	2.83	3.14	3.29

Table 3.10 Results of distance estimation using linear regression (Cont.).

	Estimated distances				
	60 cm	65 cm	70 cm	75 cm	80 cm
Mean average distance (cm)	57.54	63.43	69.56	73.96	77.83

The results showed that the accuracy of the linear regression was 95.98%. The MAE and the standard deviation were 2.78 and 3.29 cm, respectively.

The eye gaze distance can be modelled by the logarithmic regression. The solution is defined as

$$y = -27.35\ln(x) + 264.59 . \quad (3.7)$$

The test results are shown in Table 3.11

Table 3.11 Results of distance estimation using logarithmic regression.

	Estimated distances					
	60 cm	65 cm	70 cm	75 cm	80 cm	Average
Accuracy (%)	94.43	96.30	96.47	96.34	96.08	95.33
MAE (cm)	2.96	2.65	2.42	2.53	2.85	2.68
SD (cm)	2.55	2.85	2.93	3.34	3.72	3.08

	Estimated distances				
	60 cm	65 cm	70 cm	75 cm	80 cm
Mean average distance (cm)	59.08	63.48	68.95	73.72	78.63

The eye gaze distance equation obtained by using the power regression for equation can be represented as

$$y = 1143.4x^{-0.393} . \quad (3.8)$$

The test results of power regression are shown in Table 3.12.

Table 3.12 Results of distance estimation using power regression.

	Estimated distances					
	60 cm	65 cm	70 cm	75 cm	80 cm	Average
Accuracy (%)	97.03	96.53	96.36	96.12	95.79	96.37
MAE (cm)	2.01	2.33	2.49	2.85	3.26	2.59
SD (cm)	2.20	2.68	3.04	3.58	4.05	3.11

	Estimated distances				
	60 cm	65 cm	70 cm	75 cm	80 cm
Mean average distance (cm)	59.82	63.82	69.00	73.82	79.17

From the aforementioned results, the exponential regression, among the others, attained the best performance which yielded 96.69 % accuracy, 2.82 cm standard deviation, and 2.33 cm MAE. Meanwhile, the linear regression method gave 95.98% accuracy, 3.08 cm standard deviation, and 2.68 cm MAE. The power regression method showed 96.37% accuracy, 3.11 cm standard deviation, and 2.59 cm MAE.

The proposed method using the eigenvalues of the iris for eye gaze distance estimation was more accurate than the one using the summation of gray-level intensity of image patches. Therefore, the proposed method can perform the eye gaze distance estimation with a high accuracy, low standard deviation, and low MAE.

However, it is challenging to overcome the eye gaze distance for the condition under the participant's head movements. Particularly, when the participant's head tilted to the left or right of the screen, the accuracy of a distance estimation decreases. Therefore, more information was required to evaluate the eye gaze distance estimation equation. In order to improve the accuracy of eye gaze distance estimation, a novel method was required to estimate a distance between the participant's head and the screen. There was an alternative method that could be used for estimating the eye gaze distance estimation equation by using the iris area. The details of the next proposed method are described in the next section.

### 3.9.3 Eye gaze distance estimation based on iris area

An object image and focal distance relationship is illustrated in Figure 3.19 [44]. The object height is defined as  $h_o$ . And let  $d_o$  represents a distance from the object to the lens, and  $f$  refers to the focal length. In the image plane,  $h_i$  is the object height and  $d_i$  is the distance between the lens and object in the image plane. The formula of the object image and the focal distance can be described as follows:

$$\frac{d_o}{d_i} = \frac{f}{d_i - f} \quad (3.9)$$

$$\frac{1}{f} = \frac{1}{d_i} + \frac{1}{d_o} \quad (3.10)$$

and

$$\frac{d_o}{d_i} = \frac{h_o}{h_i} \quad (3.11)$$

$$h_i = \frac{h_o d_i}{d_o}$$

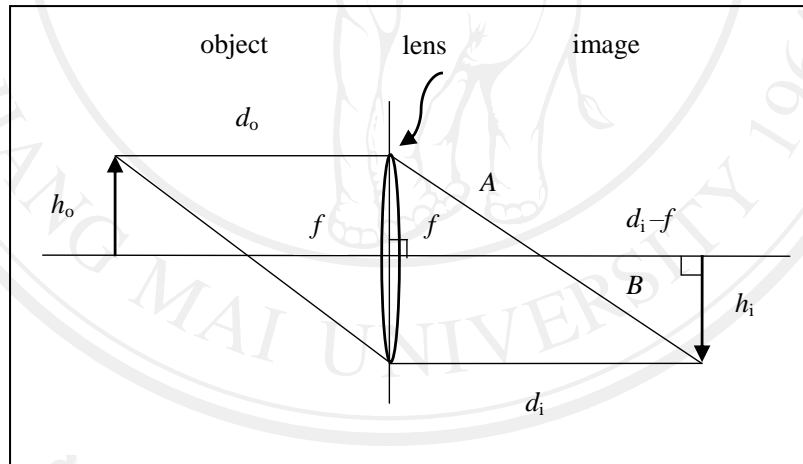


Figure 3.19 Object image and focal distance relationship.

The change of the iris area with respect to the change in distance is non-linear. However, it is still tempting to model the eye gaze distance estimation equation with the linear and non-linear regression methods. In order to evaluate the performance of an eye gaze distance estimation equation, four regression methods such as exponential, linear, logarithmic, and power regression methods were conducted to evaluate the accuracy of an equation.

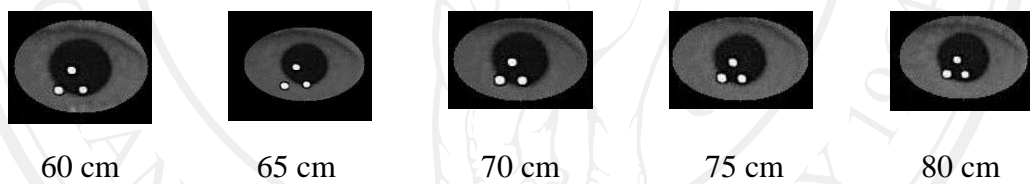
### 1) The iris area computation for a training set

Both eyes of a user were conducted to construct the eye gaze distance estimation equation. The iris area of the segmented left-right eye image could be computed. The iris radius was defined as  $r$  and was used for the iris area computation. The iris area computation can be obtained from the solution defined as follows:

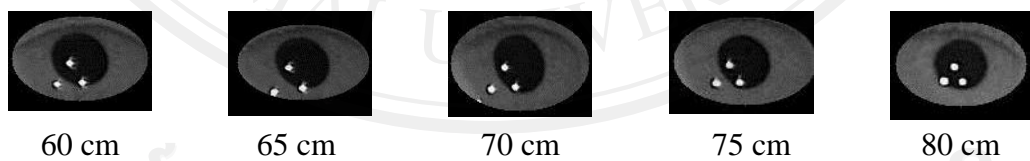
$$Area = \pi r^2 \quad (3.12)$$

where  $r$  is the longest iris radius.

The input images for training the system were obtained from the right and left eye images while the participant's head was tilted to the left of the screen. The Hough ellipse transforms method was used to segment the iris from the eye images. Therefore, the longest line of an ellipse was used for computing the iris area as presented in Figure 3.11 (a). The samples of segmented iris images used for a training set are illustrated in Figure 3.20.



(a) Right eye irises.



(b) Left eye irises.

Figure 3.20 Segmented right-left iris images.

Some examples of the resulted iris area computation were demonstrated in Table 3.13. The proposed method used the average of both iris areas for constructing the eye gaze distance estimation equation. Figure 3.21 shows the results of the iris area from different distances, ranging from 60 to 80 cm.

The training processes were constructed for four regression methods (i.e. exponential, linear, logarithmic, and power regressions). The results of exponential regression for the iris area are presented in Figure 3.21 and are defined as

$$y = 96.378e^{-0.00003x} \quad (3.13)$$

where  $y$  is the eye gaze distance and  $x$  is the average iris area.

Table 3.13 Examples of iris area of both eyes at distance of 60 cm.

Image positions	Iris radius		Iris area		Average of area (pixels)
	Left-eye	Right-eye	Left-eye	Right-eye	
1	61	64	11689.87	12867.96	12278.91
2	67	70	14102.61	15393.80	14748.21
3	65	68	13273.23	14526.72	13899.98
4	64	68	12867.96	14526.72	13697.34
5	67	74	14102.61	17203.36	15652.99
6	65	71	13273.23	15836.77	14555.00
7	65	72	13273.23	16286.02	14779.62
8	67	70	14102.61	15393.80	14748.21
9	65	60	13273.23	11309.73	12291.48

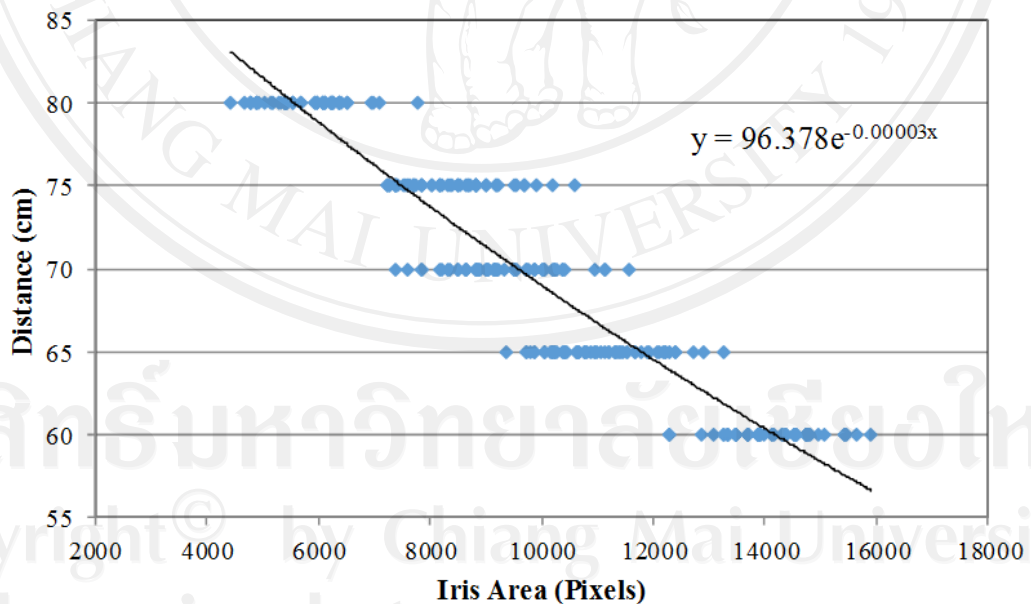


Figure 3.21 Average iris area at the distance between 60 and 80 cm.

The solution of the linear regression for eye gaze distance estimation is represented as follows:

$$y = 92.537 - 0.0023x . \quad (3.14)$$

The solution of the logarithmic regression is

$$y = -21.33\ln(x) + 264.87 . \quad (3.15)$$

And the solution for eye gaze distance estimation by the power regression method is

$$y = 1135.6x^{-0.306} . \quad (3.16)$$

## 2) The experimental results

The eye gaze distance estimation obtained by using the principle of iris area was validated for accuracy, mean average of distance estimation, and the standard deviation. The proposed method was tested with 30 participants. There were four regression methods (exponential, linear, logarithmic, and power regression) which were evaluated for the performance of the eye gaze distance estimation equation. In addition, the proposed method was tested under conditions when the participant's head moved to the left and right of the screen. The results of the exponential regression method when the participant's head tilted to the left of the screen are demonstrated in Table 3.14. Conversely, Table 3.15 shows the results gathered when the participant's head tilted to the right. The average results of both irises's area are presented in Table 3.16.

Table 3.14 Results of distance estimation of the exponential regression principle on the iris area of participant's head tilted to the left of the screen.

	Estimated distances					
	60 cm	65 cm	70 cm	75 cm	80 cm	Average
Accuracy (%)	96.84	97.08	97.46	97.79	97.75	97.37
SD (cm)	1.97	1.86	1.60	1.55	1.56	1.71

Table 3.14 Results of distance estimation of the exponential regression principle on the iris area of participant's head tilted to the left of the screen (Cont.).

	Estimated distances				
	60 cm	65 cm	70 cm	75 cm	80 cm
Mean average distance (cm)	60.52	65.13	70.01	74.72	79.13

Table 3.15 Results of distance estimation of the exponential regression principle on the iris area of the participant's head tilted to the right of the screen.

	Estimated distances					
	60 cm	65 cm	70 cm	75 cm	80 cm	Average
Accuracy (%)	97.17	97.21	97.32	97.74	97.96	97.48
SD (cm)	1.89	1.99	1.67	1.46	1.45	1.69

	Estimated distances				
	60 cm	65 cm	70 cm	75 cm	80 cm
Mean average distance (cm)	60.31	65.31	69.89	74.87	79.05

Table 3.16 Results of eye gaze distance estimation of average both irises area using the exponential regression.

	Estimated distances					
	60 cm	65 cm	70 cm	75 cm	80 cm	Average
Accuracy (%)	97.00	97.14	97.39	97.77	97.86	97.43
SD (cm)	1.93	1.93	1.63	1.51	1.51	1.70

	Estimated distances				
	60 cm	65 cm	70 cm	75 cm	80 cm
Mean average distance (cm)	60.42	65.22	69.95	74.80	79.09

The experimental results of the exponential regression method showed 97.43% accuracy and 1.70 standard deviation. The linear regression method was also tested and the test results are presented in Table 3.17 to Table 3.19.

Table 3.17 Results of distance estimation of the linear regression principle on the iris area of participant's head tilted to the left of the screen.

	Estimated distances					
	60cm	65cm	70cm	75cm	80cm	Average
Accuracy (%)	97.40	96.16	95.67	95.70	96.05	96.20
SD (cm)	2.48	2.20	1.76	1.60	1.52	1.91

	Estimated distances				
	60 cm	65 cm	70 cm	75 cm	80 cm
Mean average distance (cm)	56.95	62.44	67.99	73.00	77.39

Table 3.18 Results of distance estimation of the linear regression principle on the iris area of participant's head tilted to the right of the screen.

	Estimated distances					
	60 cm	65 cm	70 cm	75 cm	80 cm	Average
Accuracy (%)	93.97	95.72	96.26	96.93	96.55	95.89
SD (cm)	2.38	2.33	1.84	1.51	1.42	1.90

	Estimated distances				
	60 cm	65 cm	70 cm	75 cm	80 cm
Mean average distance (cm)	56.68	62.75	67.92	73.20	77.38

Table 3.19 Results of distance estimation of the average both irises area using the linear regression method.

	Estimated distances					
	60 cm	65 cm	70 cm	75 cm	80 cm	Average
Accuracy (%)	95.69	95.94	95.97	96.32	96.30	96.04
SD (cm)	2.43	2.27	1.80	1.55	1.47	1.90

	Estimated distances				
	60 cm	65 cm	70 cm	75 cm	80 cm
Mean average distance (cm)	56.81	62.59	67.96	73.10	77.38

In addition, the experimental results for the logarithmic regression method are presented in Table 3.20 through Table 3.22.

Table 3.20 Results of distance estimation of the logarithmic regression principle on the iris area of participant's head tilted to the left of the screen.

	Estimated distances					
	60 cm	65 cm	70 cm	75 cm	80 cm	Average
Accuracy (%)	97.40	96.16	95.67	95.70	96.05	96.20
SD (cm)	1.49	1.56	1.53	1.74	2.14	1.69

	Estimated distances				
	60 cm	65 cm	70 cm	75 cm	80 cm
Mean average distance (cm)	59.09	62.77	67.13	72.02	77.52

Table 3.21 Results of distance estimation of the logarithmic regression principle on the iris area of participant's head tilted to the right of the screen.

	Estimated distances					
	60 cm	65 cm	70 cm	75 cm	80 cm	Average
Accuracy (%)	97.32	96.38	95.79	96.11	96.30	96.38
SD (cm)	2.38	2.33	1.84	1.51	1.42	1.90

	Estimated distances				
	60 cm	65 cm	70 cm	75 cm	80 cm
Mean average distance (cm)	56.68	62.75	67.92	73.20	77.38

Table 3.22 Results of distance estimation of the average both irises area using logarithmic regression method.

	Estimated distances					
	60 cm	65 cm	70 cm	75 cm	80 cm	Average
Accuracy (%)	97.36	96.27	95.73	95.91	96.18	96.29
SD (cm)	1.47	1.62	1.55	1.69	2.04	1.67

	Estimated distances				
	60 cm	65 cm	70 cm	75 cm	80 cm
Mean average distance (cm)	59.03	62.88	67.12	72.14	77.46

Finally, the experimental results for eye gaze distance estimation obtained from the power regression method are presented in Table 3.23 and Table 3.25

Table 3.23 Results of distance estimation of the power regression principle on the iris area of participant's head tilted to the left of the screen.

	Estimated distances					
	60 cm	65 cm	70 cm	75 cm	80 cm	Average
Accuracy (%)	97.83	65.99	95.07	95.01	95.68	95.92
SD (cm)	1.29	1.42	1.46	1.77	2.34	1.66

	Estimated distances				
	60 cm	65 cm	70 cm	75 cm	80 cm
Mean average distance (cm)	59.35	62.55	66.64	71.47	77.27

Table 3.24 Results of distance estimation of the power regression principle on the iris area of participant's head tilted to the right of the screen.

	Estimated distances					
	60 cm	65 cm	70 cm	75 cm	80 cm	Average
Accuracy (%)	97.89	96.25	94.88	95.20	95.88	96.02
SD (cm)	1.24	1.55	1.50	1.67	2.12	1.62

Table 3.24 Results of distance estimation of the power regression principle on the iris area of participant's head tilted to the right of the screen (Cont.).

	Estimated distances				
	60 cm	65 cm	70 cm	75 cm	80 cm
Mean average distance (cm)	59.23	62.78	66.61	71.71	77.16

Table 3.25 Results of distance estimation of the average both irises area using the power regression method.

	Estimated distances					
	60 cm	65 cm	70 cm	75 cm	80 cm	Average
Accuracy (%)	97.86	96.12	94.98	95.11	95.78	95.97
SD (cm)	1.27	1.48	1.48	1.72	2.23	1.64

	Estimated distances				
	60 cm	65 cm	70 cm	75 cm	80 cm
Mean average distance (cm)	59.29	62.67	66.63	71.59	77.22

In summary, the experiment was performed on 30 participants to validate the eye gaze distance estimation equation. The eye gaze images were obtained when the participant's head moved to the left and right of the screen. The test results for eye gaze distance estimation of the exponential regression method with the head movement to the left and right of the screen showed 97.43% average accuracy, and 1.70 cm average standard deviation. The linear regression method showed the 96.04% average accuracy with 1.90 cm average standard deviation, and the logarithmic method showed 96.29% average accuracy with 1.90 cm average standard deviation. Meanwhile, the results of the power regression showed 95.97% average accuracy, and 1.64 cm average standard deviation. Therefore, the best method is clearly the exponential one because of its highest accuracy and lowest standard deviation. The exponential method was then selected for the eye gaze distance estimation and was used in the eye gaze estimation.

### 3.10 Eye gaze center detection

The iris has an aperture stop known as the pupil lying at the center of the iris. The pupil center is equivalent to the eye gaze center or the visual axis of the human's eye. While the participant is looking at different points on the screen, the eye gaze center changes with respect to the positions on the screen. Therefore, the pupil center is required to determine the relationship between the eye gaze center and the positions on the screen at which the participant is looking. An example of eye gaze center detection is shown in Figure 3.22.

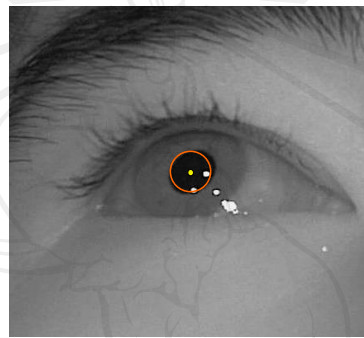


Figure 3.22 Eye gaze center.

In practice, the pupil image is not always a circular shape. It can also be an elliptical shape. Thus, the eye gaze center detection which uses the Hough circle method can cause an error in the eye gaze center detection. Therefore, the accuracy of eye gaze center detection was improved by using the principle of the eigenvector instead of using the Hough circle transform. The segmented eye image had an approximate size of  $100 \times 100$  pixels. The eye gaze center and eye gaze displacements could be determined from the image as presented in Figure 3.23. The eigenvalue method was conducted to compute the eye gaze center. The proposed method can be described as follows:

Copyright© by Chiang Mai University  
All rights reserved

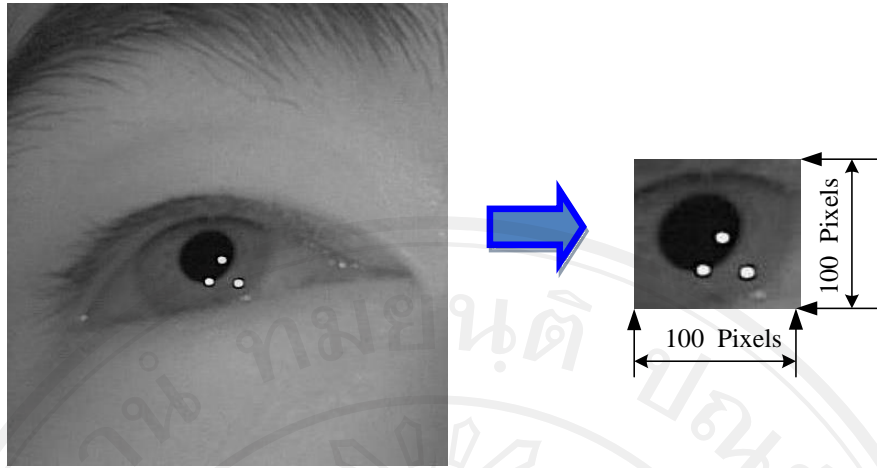


Figure 3.23 Input images for eye gaze center detection.

The eye gaze center computation can be described as follows:

1. Use an eye gaze image as shown in Figure 3.24.
2. Transform the RGB image to a binary image.
3. Determine the eye gaze image size  $[i_x, j_y]$

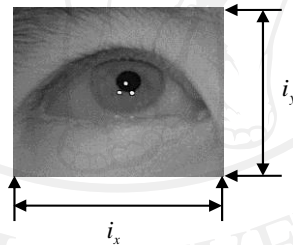


Figure 3.24 Eye image for gaze center detection.

4. Perform image thresholding of the pupil color as presented in Figure 3.25 where the brightness is selected for computing the eye gaze center.

ลิขสิทธิ์มหาวิทยาลัยเชียงใหม่  
 Copyright © by Chiang Mai University  
 All rights reserved



Figure 3.25 A binary of pupil image.

5. Compute the mean average vector of the pupil positions by

$$m_x = \frac{1}{k} \sum_{k=1}^k x_k \quad (3.17)$$

where  $x_k$  is the vector positions  $[i_x, j_y]$  and  $k$  is the number of vector positions in the pupil image.



Figure 3.26 Eye gaze center computation.

### 3.11 Pupil-glint vector computation

The pupil-glint vector is related to the displacements and direction between the pupil center and the reference point on the cornea. The eye gaze center could be determined by using the eigenvector computations, and the glint was detected by using the Blob coloring for image labelling.

The proposed system was tested by using two-point and three-point light sources for illuminating on the participant's cornea. The cornea was reflected by two point light sources as shown in Figure 3.27. Then, the position of two-point light sources for the both eyes could be defined, according to  $\vec{P}_1^{right}$ ,  $\vec{P}_2^{right}$ ,  $\vec{P}_1^{left}$ , and  $\vec{P}_2^{left}$ . Displacements between two glints position are called the 'inter-glnt' distances. The midpoint of the inter-glnt distance is defined as the center reference for eye gaze displacements and

pupil vector computation. Thus, the midpoint of both eyes is denoted by  $\vec{G}_c^{right}$ , and  $\vec{G}_c^{left}$ . The midpoint of the inter-glint distance can be defined as follows:

$$\vec{G}_c^{right} = \frac{1}{2} |\vec{P}_1^{right} - \vec{P}_2^{right}| \quad (3.18)$$

$$\vec{G}_c^{left} = \frac{1}{2} |\vec{P}_1^{left} - \vec{P}_2^{left}| \quad (3.19)$$

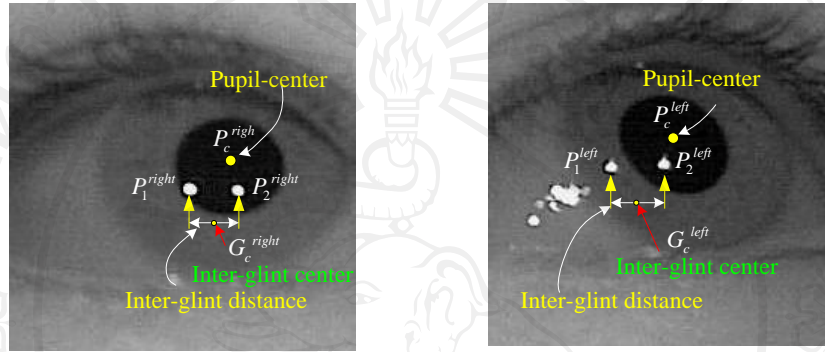


Figure 3.27 Pupil centers and inter-glint distances.

Two point light sources were located at the bottom of the screen. Therefore, they reflected on the cornea and were used as the reference lower position of the screen. The center of pupil is defined as  $\vec{P}_c^{right}$  and  $\vec{P}_c^{left}$  for the right and left eyes, respectively. These centers are also used for eye gaze displacement computations. The pupil-glint vector can be calculated as follows:

$$\vec{PG}_{right-eye} = \vec{P}_c^{right} - \vec{G}_c^{right}, \text{ and } \vec{PG}_{left-eye} = \vec{P}_c^{left} - \vec{G}_c^{left} \quad (3.20)$$

where  $\vec{PG}_{right-eye}$  and  $\vec{PG}_{left-eye}$  are the pupil-glint vectors, the  $\vec{G}_c^{right}$  and  $\vec{G}_c^{left}$  are inter-glint centers of the right and left eyes, respectively.

The average of the pupil-glint vector is used for mapping the eye gaze displacements to the screen positions. These results can give the accurate eye gaze points on the screen positions estimation. The formula of average pupil-glint vector is represented as follows:

$$\overline{\mathbf{PG}}_{avg} = \frac{1}{2} \left( \left( \overline{\mathbf{P}}_c^{right} - \overline{\mathbf{G}}_c^{right} \right) + \left( \overline{\mathbf{P}}_c^{left} - \overline{\mathbf{G}}_c^{left} \right) \right). \quad (3.21)$$

Therefore, this experiment used two and three infrared light sources where the reference points for each case are shown in Figure 3.28.

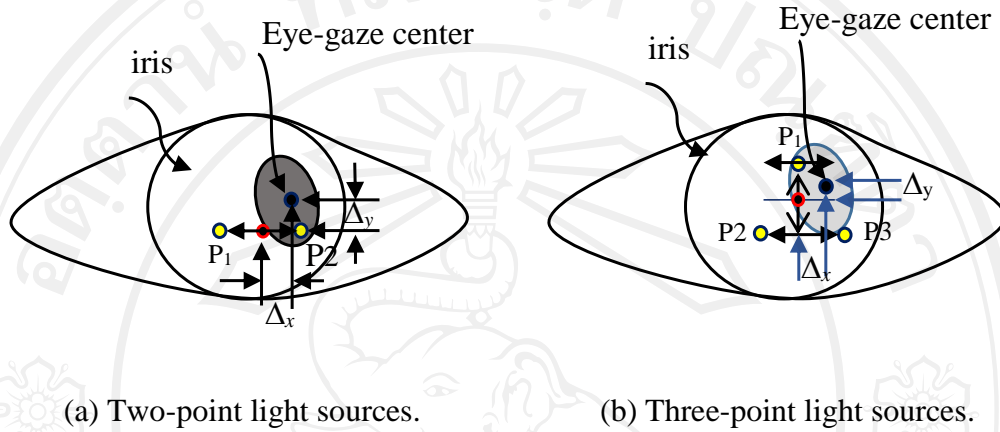


Figure 3.28 Reference points of infrared light sources on the cornea.

Figure 3.28 (b) presents the reference point from the three near-infrared light sources reflected on the cornea. The center point between the glint position of P<sub>1</sub>, P<sub>2</sub>, and P<sub>3</sub> is set up for the screen center reference and used for eye gaze displacements computation. The displacements can be computed according to (3.20) and (3.21).

After the pupil-glint vector is computed, the eye gaze displacements can be obtained from the average of both eye gaze displacements. The eye gaze displacements are defined as  $\Delta_x^{right}$ ,  $\Delta_y^{right}$ ,  $\Delta_x^{left}$  and  $\Delta_y^{left}$  of the right-left eye in horizontal and vertical axes. The formula of the average of both eyes-gaze displacements can be written as follows:

$$D_x^{disp} = \frac{1}{2} \left| \Delta_x^{right} + \Delta_x^{left} \right| \quad (3.22)$$

$$D_y^{disp} = \frac{1}{2} \left| \Delta_y^{right} + \Delta_y^{left} \right| \quad (3.23)$$

where  $D_x^{disp}$  is the average of eyes-gaze displacements on the horizontal axis and  $D_y^{disp}$  is the average eye gaze displacements on the vertical axis.

### 3.12 Three-dimensional eye model

The three dimensional (3-D) model of the human eye is more useful than two dimensional (2-D) models in eye gaze mapping to the computer screen positions. Previously, two dimensional (2-D) eye gaze images were used for mapping the eye gaze displacements. However, the results from two dimensional methods provide low resolution. If the participant's head moves, the system unavoidably requires re-calibration. Therefore, using the 3-D eye model is more accurate than using the 2-D images because the information of the depth can be utilized for compensating gaze mapping to the screen positions. Since the distance between the participant's head and the screen position can be calculated and the 2-D eye gaze image is known, the real-world iris and eyeball radii can also be calculated. Thus, the 3-D eye model is used for eye gaze mapping to the computer screen positions.

Before 3-D eye modeling a human eye structure has been considered as shown in Figure 3.29. The structure can be divided into two parts: the anterior cornea and the posterior sclera [15], [45]. The cornea shape is the sphere with the radius of the curvature approximately equal to 8 mm. The radius of the curvature for the sclera is about 12 mm.

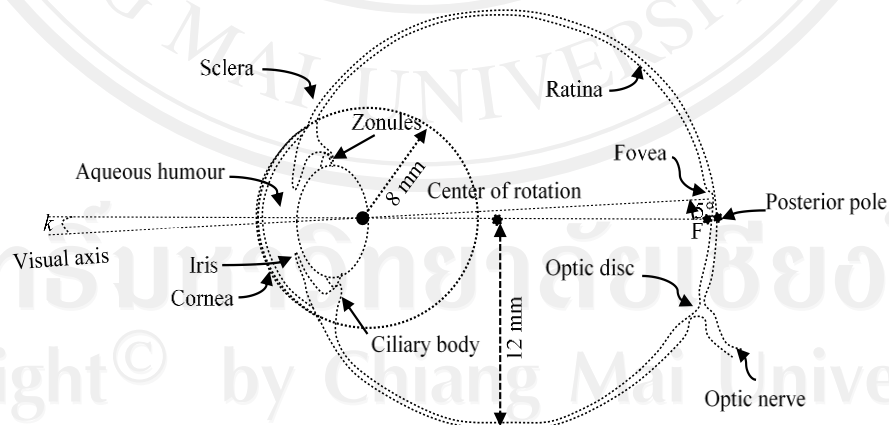


Figure 3.29 Human eye structures.

As represented in Figure 3.29, the optic axis of the eye is a line joining the center curvatures and the reflecting surfaces. The angle between optical and visual axes is the Kappa angle. The pupil center is defined as the center of the visual axis of the human eye.

Consequently, the three dimensional eye can be modeled as presented in Figure 3.30. The optic axis of the eye model is the pupil center line. The visual angles on the horizontal and vertical axes are defined as  $\alpha$  (around the  $OZ$  axis) and  $\beta$  (around the  $OY$  axis). The visual angle is utilized for calculating the eye gaze point on the screen. The actual iris radius of the eye model can be calculated by using inverse perspective transformation [37]. The iris radius is determined from a single eye image. The results from the iris radius calculation are used for computing the eyeball radius. According to the method proposed in [26], it is computed by using the ratio of  $R/r$  equal to 2.

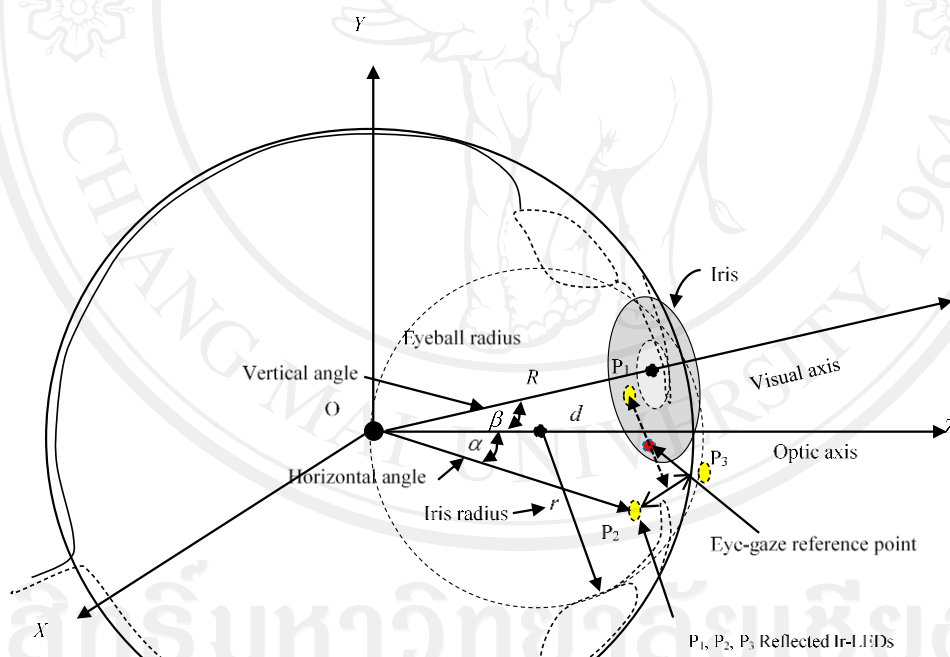


Figure 3.30 Three-dimensional eye models.

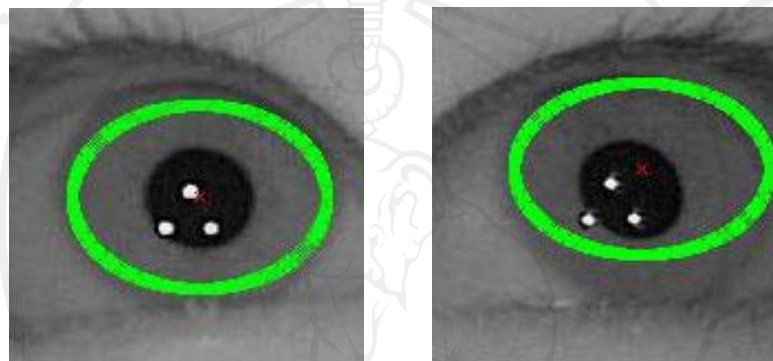
The visual angle measurement is obtained by using the eye gaze displacements and eyeball radius. As shown in Figure 3.30, the distance from the eye gaze center of the iris

is defined as  $d$ , the eyeball radius is defined as  $R$ , and iris radius is defined as  $r$ . Therefore, the relation between  $R$ ,  $d$ , and  $r$  becomes

$$R^2 = d^2 + r^2 \quad (3.24)$$

where  $d$  is a distance from the eyeball center to the cornea surface.  $R$  is the eyeball radius and  $r$  is the iris radius.

The iris radius was determined by applying the Hough ellipse method. An example of iris detection for both eyes is presented in Figure 3.31.



(a) Iris radius detected of right eye. (b) Iris radius detected of left eye.

Figure 3.31 Example of iris radius detected using the Hough ellipse.

### 3.13 Visual angle of eye gaze estimation

Figure 3.32 presents the geometry of the eye-model reflected by the point light sources. Here, the inter-glinc distance centers were set up as the reference points which were used for computing the eye gaze displacements of the eye gaze center. After the distance between the inter-glinc center and the eye gaze center had been calculated, the iris radius was determined. Then, the 3-D eye model was used for computing the visual angle of the eye at which the participant was looking at the screen. The visual angle is composed of the horizontal  $\alpha$ -angle and vertical  $\beta$ -angle. Therefore, the most important factor of the eye model is the eyeball radius because it is used for eye gaze visual angle computation.

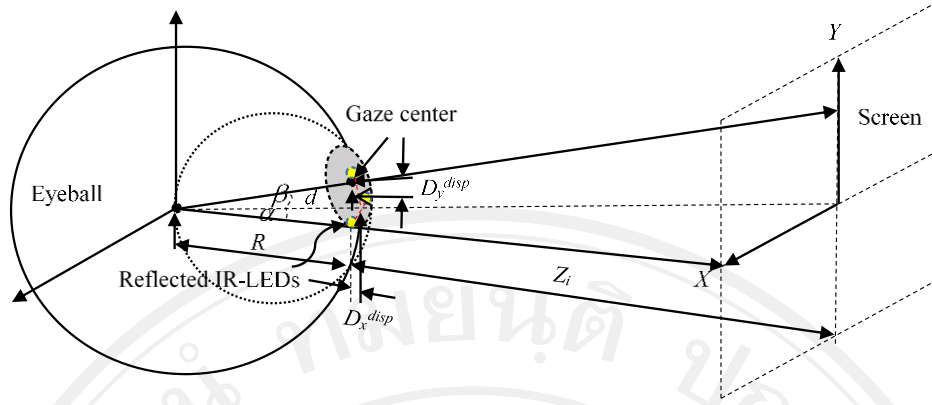


Figure 3.32 Geometry of the eye gazing to the screen.

As shown in Figure 3.32, the real-world eye gaze displacements are defined by  $D_x^{disp}$  and  $D_y^{disp}$ . Then, the formula of the visual eye gaze angle on the vertical axis can be written as follows:

$$\beta = \tan^{-1} \left( \frac{D_y^{disp}}{d} \right). \quad (3.25)$$

The horizontal visual eye gaze angle is represented by

$$\alpha = \tan^{-1} \left( \frac{D_x^{disp}}{d} \right). \quad (3.26)$$

where  $D_x^{disp}$  and  $D_y^{disp}$  are the average of eye gaze displacements,  $d$  is the eyeball radius and  $Z_i$  is the distance between the face and the computer screen.

The distance of the eye gaze point on the computer screen can be computed according to (3.25) and (3.26) and the displacements,  $D_x^{disp}$  and  $D_y^{disp}$ , can be changed by  $X$  and  $Y$ , respectively. After the visual eye gaze angle has been computed, the distance on the computer screen can be expressed as follows:

$$\beta = \tan^{-1} \left( \frac{Y}{Z_i + d} \right), \quad (3.27)$$

and

$$\alpha = \tan^{-1} \left( \frac{X}{Z_i + d} \right). \quad (3.28)$$

From (3.27) and (3.28), the actual distances of eye gaze on the computer screen are determined and can be described by the equation,

$$Y = (Z_i + d) \tan \beta, \quad (3.29)$$

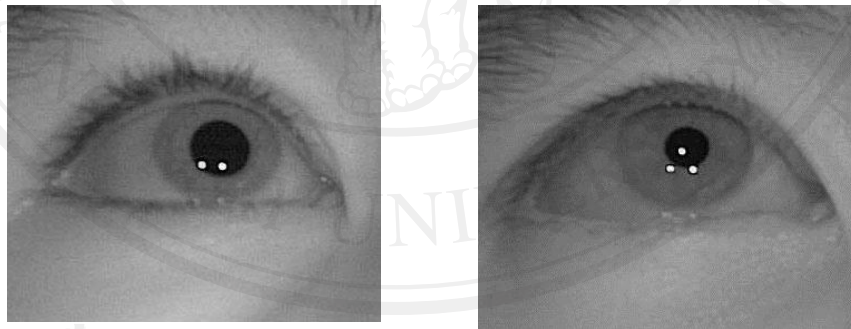
and

$$X = (Z_i + d) \tan \alpha. \quad (3.30)$$

Before the computed actual screen was used for mapping to the computer screen position, it was necessary to check for the direction of both eyes. The details of eye gaze mapping to the screen are described in the next section.

### 3.14 Eye gaze mapping to screen

Gaze direction is obtained by the pupil-glint vector computation process. There are two configurations of IR-LEDs used in the experiment: two infrared light sources and three infrared light sources. The results of near-infrared light sources reflected on the cornea for both configurations are presented in Figure 3.33.



(a) Two IR-LEDs.

(b) Three IR-LEDs.

Figure 3.33 Result of IR-LEDs reflected on the cornea.

#### 3.14.1 Eye gaze mapping to screen using two IR-LEDs light sources

The two point light sources on the cornea images with respect to  $P_1$  and  $P_2$  as shown in Figure 3.34. The inter-glinc center is set as the reference center of the computer screen. The pupil-glinc vector used for considering map the eye gaze displacements to the

screen. The screen width is defined as  $w$ , the screen height is defined as  $h$ , and the half width of the screen is defined as  $w/2$ .

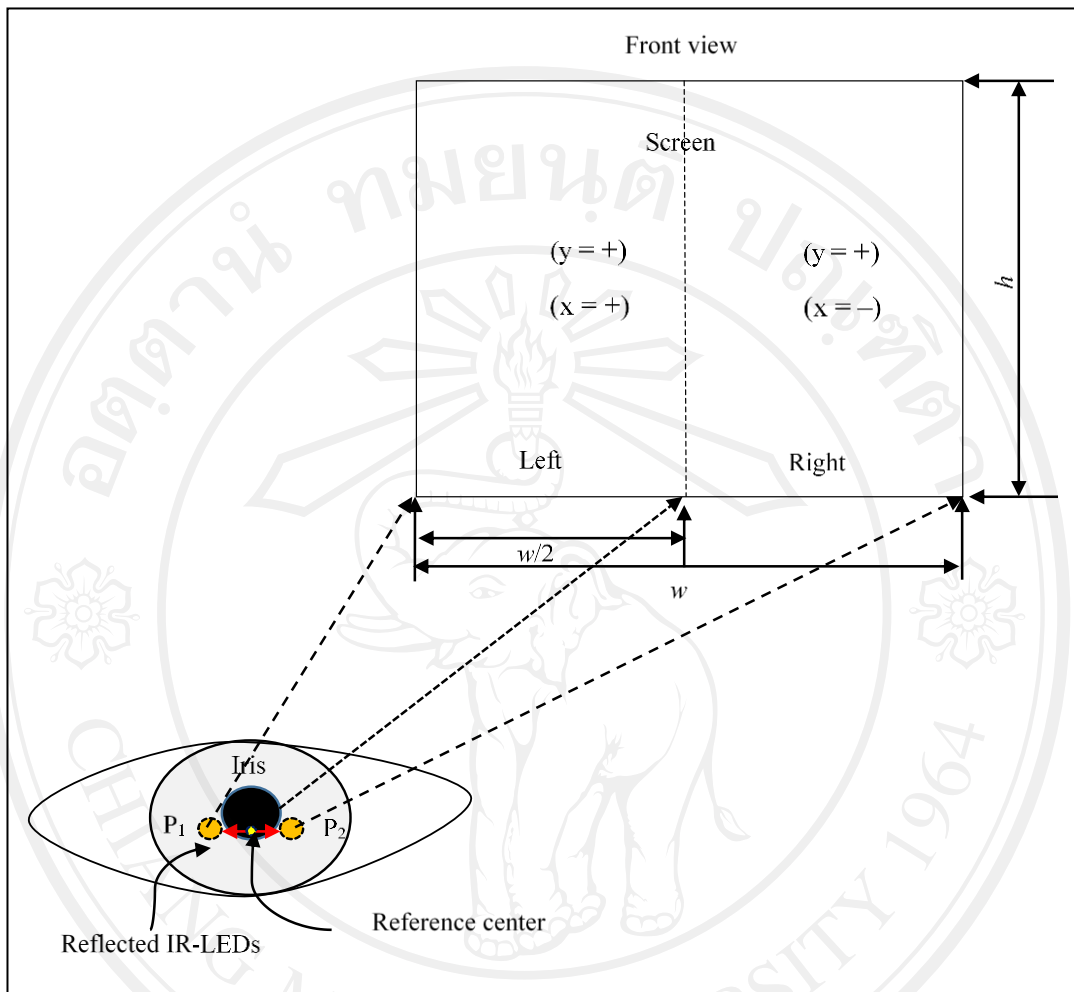


Figure 3.34 Screen mapping condition by using two IR-LEDs.

### 3.14.2 Eye gaze mapping to screen using three IR-LEDs light sources

The cornea reflected by the three IR-LEDs is illustrated in Figure 3.35. Using three IR-LEDs makes screen mapping easier since the reference point is the midpoint between the positions of  $P_1$  through  $P_3$ . From Figure 3.35, the points  $P_1$  and  $P_2$  from the eye gaze image are set up at the bottom of the computer screen while the point  $P_3$  is set up on the top center of the screen. Meanwhile, the center between three point light sources from the eye gaze image is referred as the screen center. Before mapping the eye gaze displacements to the screen coordinate, the eye gaze vector can be obtained from (3.20).

The pupil-glint vectors or directions of the eye gaze image can be defined as shown in Figure 3.35.

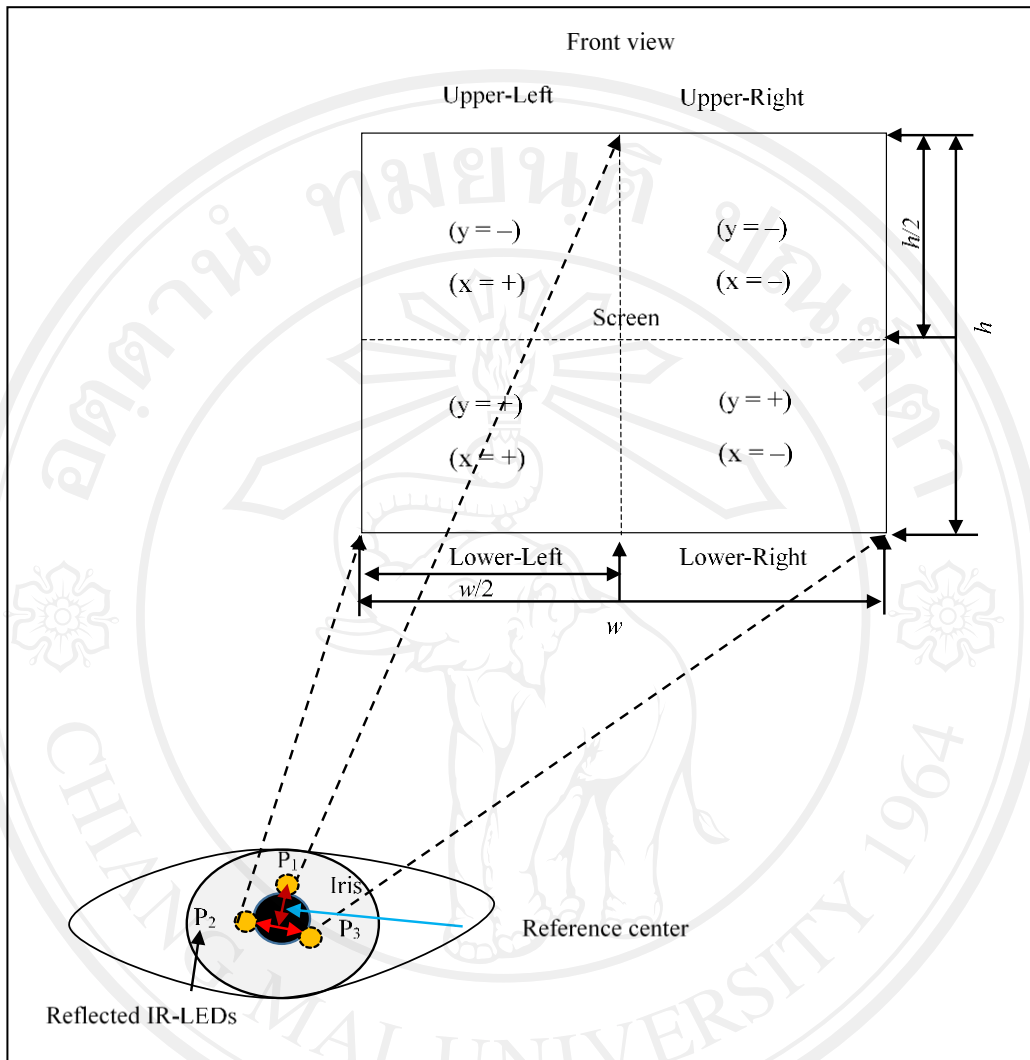


Figure 3.35 Screen mapping using three IR-LEDs.

### 3.15 Eye gaze distance transform to the computer screen

The results from eye gaze distance computation were obtained by using (3.29) and (3.30). The direction of eye gaze point was required to be checked before mapping to the screen position. The method to compute the screen coordinate for two near IR-LEDs can be described as follows:

### 3.15.1 Condition and terms for two near IR-LEDs

1) **When the participant looks at the left side of the screen:**

$$\begin{aligned}\text{Screen coordinate} &= X \text{ (cm)} && \text{for the horizontal axis} \\ &= Y \text{ (cm)} && \text{for the vertical axis}\end{aligned}$$

2) **When the participant looks at the right side of the screen:**

$$\begin{aligned}\text{Screen coordinate} &= (w/2) + X \text{ (cm)} && \text{for the horizontal axis} \\ &= Y \text{ (cm)} && \text{for the vertical axis}\end{aligned}$$

For the three IR-LEDs configuration as shown in Figure 3.34, the screen coordinate condition is explained as follows:

### 3.15.2 Condition and terms for three near IR-LEDs

1) **When the participant looks at the upper-left side of the screen:**

$$\begin{aligned}\text{Screen coordinate} &= (w/2) - X \text{ (cm)} && \text{for the horizontal axis} \\ &= (h/2) + Y \text{ (cm)} && \text{for the vertical axis}\end{aligned}$$

2) **When the participant looks at the upper-right side of the screen:**

$$\begin{aligned}\text{Screen coordinate} &= (w/2) + X \text{ (cm)} && \text{for the horizontal axis} \\ &= (h/2) + Y \text{ (cm)} && \text{for the vertical axis}\end{aligned}$$

3) **When the participant looks at the lower-left side of the screen:**

$$\begin{aligned}\text{Screen coordinate} &= (w/2) - X \text{ (cm)} && \text{for the horizontal axis} \\ &= (h/2) - Y \text{ (cm)} && \text{for the vertical axis}\end{aligned}$$

4) **While the participant looks at the lower-right side of the screen:**

$$\begin{aligned}\text{Screen coordinate} &= (w/2) + X \text{ (cm)} && \text{for the horizontal axis} \\ &= (h/2) - Y \text{ (cm)} && \text{for the vertical axis}\end{aligned}$$

### 3.16 Screen position for experiment

The screen positions for eye gaze tracking on the screen are divided into 10 columns and 6 rows. The test points are specified as the screen coordinate  $(y, x)$  positions in the pixel unit. Here, the computer screen with resolutions of  $1024 \times 768$  pixels was used for the experiment. The actual screen position is shown in Figure 3.36.

$(y, x)$									
(674.13, 63.24)	(674.13, 156.64)	(674.13, 265.03)	(674.13, 367.43)	(674.13, 469.83)	(674.13, 572.23)	(674.13, 668.61)	(674.13, 774.02)	(674.13, 876.42)	(674.13, 972.8)
(583.11, 63.24)	(583.11, 156.64)	(583.11, 265.03)	(583.11, 367.43)	(583.11, 469.83)	(583.11, 572.23)	(583.11, 668.61)	(583.11, 774.02)	(583.11, 876.42)	(583.11, 972.8)
(460.79, 63.24)	(460.79, 156.64)	(460.79, 265.03)	(460.79, 367.43)	(460.79, 469.83)	(460.79, 572.23)	(460.79, 668.61)	(460.79, 774.02)	(460.79, 876.42)	(460.79, 972.8)
(327.11, 63.24)	(327.11, 156.64)	(327.11, 265.03)	(327.11, 367.43)	(327.11, 469.83)	(327.11, 572.23)	(327.11, 668.61)	(327.11, 774.02)	(327.11, 876.42)	(327.11, 972.8)
(199.11, 63.24)	(199.11, 156.64)	(199.11, 265.03)	(199.11, 367.43)	(199.11, 469.83)	(199.11, 572.23)	(199.11, 668.61)	(199.11, 774.02)	(199.11, 876.42)	(199.11, 972.8)
(71.11, 63.24)	(71.11, 156.64)	(71.11, 265.03)	(71.11, 367.43)	(71.11, 469.83)	(71.11, 572.23)	(71.11, 668.61)	(71.11, 774.02)	(71.11, 876.42)	(71.11, 972.8)

Figure 3.36 Screen position used in experiment.